AIAA JOURNAL
Vol. 41, No. 4, April 2003

Passive Mixing Control via Lobed Injectors in High-Speed Flow

A. J. Majamaki,* O. I. Smith,† and A. R. Karagozian‡
University of California, Los Angeles, Los Angeles, California 90095-1597

The near-field flow and mixing characteristics of nonreactive lobed fuel injectors in subsonic and transonic airstreams were studied experimentally. Three alternative injector geometries were explored, two of which had lobed shapes. These lobed injectors mixed gas-phase injectant (nitrogen) and coflowing air to different extents, straining fluid interfaces due to streamwise vorticity generation. The experiments were conducted in a "trisonic" wind tunnel, with coflowing airstream Mach numbers ranging from 0.4 to 1.2. Visualization of the downstream evolution of the injectant was achieved via planar laser-induced fluorescence imaging of acetone seeded in the nitrogen. Comparisons of near-field flow evolution, mixing properties, and scalar dissipation and strain rates were made among different injectors for the different experimental flow conditions. It was observed that lobed injector geometries produced greater near-field mixing as well as higher effective interfacial strain rates than nonlobed injectors in the subsonic (Mach 0.4) regime, although at higher subsonic Mach numbers mixing increases were accompanied by a reduction in the effective strain rate. Flow evolution observed in the experiments was also compared with numerical simulations of vorticity evolution and rollup, with good correspondence.

Introduction

AMONG the goals of the present study is the examination and quantification of the effects of passively controlled injectant–air mixing, as created by specific fuel injector geometries, for operation in subsonic and transonic flow. This study is part of a larger program that has examined mixing and combustion characteristics associated with lobed fuel injectors.[1–4] The lobed fuel injector, shown schematically in Fig. 1, is a device in which rapid initial mixing of reactants can occur through streamwise vorticity generation. In low-speed (essentially incompressible) flow, the device is known to produce high strain rates, which can enhance mixing while delaying ignition at fuel–air (or injectant–air) interfaces.[1,3,4]

The lobed injector in general consists of two parallel, corrugated plates that are flat at the upstream edge and have a ramp angle α representing the downstream spatial growth of the corrugation. Fuel or other injectant is introduced from between the plates into coflowing air. Streamwise vorticity is created in the lobed injector by the oppositely oriented secondary flows that develop along the sides of each of the lobes; these flows eventually roll up into counter-rotating vortical structures oriented in the streamwise direction. This vorticity rollup regime is coincident with a region in which fuel and air can mix rapidly. In subsonic flows, when the strain rates relax farther downstream, ignition of potentially lean, premixed flame structures can occur[3,4] providing conditions under which temperature-sensitive combustion byproducts such as NO may be reduced.

The mechanism for rollup in the lobed injector is the same as that for the single-interface lobed mixer[5–9] studied extensively for its applications to turbofan mixing and studied to a more limited degree for its combustion applications.[10–12] To achieve noise reduction in supersonic mixer/ejectors, lobed shaped nozzles have been found to produce mixing enhancement as a consequence of the streamwise vorticity generation.[13,14] This observation is significant in that degradation of mixing in supersonic free shear layers, in contrast to subsonic shear layers, is well recognized.[15,16] In supersonic flow, the lobed mixer's potential core length is seen to be reduced by a factor of two, with an increase in ejector pumping by as much as 75% when compared with a conventional conical mixer.[13,14] For application as a supersonic fuel nozzle for a dual-combustion ramjet, recent studies[17–19] suggest that the "petal" or lobed shaped nozzle increases mixing above that seen for a conical nozzle through creation of a more uniform temperature profile downstream of the coaxial mixing zone. However, detailed diagnostics for this flowfield, especially for the reacting case, have not been performed, and as a consequence, the notion of and mechanism for enhanced supersonic mixing is not as extensively quantified for the petal nozzle.

Recent mixing studies by our group at the University of California, Los Angeles (UCLA), have focused on both reactive and nonreactive lobed injector flowfields but at very low speeds (Mach 0.05 or less) of the gaseous injectant and air coflow. Experimental studies of the nonreactive lobed injector flowfield[1] indicate increases in molecular mixing and scalar dissipation rates or strain rates as compared with a planar geometry for a range of flow conditions. These studies employ planar laser-induced fluorescence (PLIF) imaging of acetone seeded in the injectant (CO_2) to quantify local unmixedness and average scalar dissipation rates, from which strain rates are estimated.[20] Corresponding computations of the lobed injector flowfield[2] allow prediction, via vortex element simulations, of the evolution of the injectant, with good qualitative as well as quantitative correspondence to nonreactive experiments. Recent experiments in a low-speed reactive flowfield[3,4] compare the behavior of different lobed and nonlobed injector flowfields, specifically monitoring the sensitivities of NO_x and CO emissions to the global equivalence ratio as well as examining the beneficial effects of confinement of the crossflow.

The present lobed injector experiments were conducted in the absence of a chemical reaction, with nitrogen as the injectant introduced into a compressible (subsonic and transonic) coflowing airstream. It was sought to examine experimentally and quantify accurately the near-field mixing characteristics of the lobed fuel injector in a nonreactive, high-speed flowfield, to see whether enhanced mixing continued from the subsonic into the transonic regime. Beyond mixing, scalar dissipation rate as well as strain rate data were extracted to enable an understanding of the potential for ignition delay by the lobed injector at higher speeds. Whereas ignition delay may be desirable in the lower subsonic regime with respect to the potential for lowered NO_x emissions, in the higher subsonic regime and above, both mixing and combustion processes must take place very rapidly, so that ignition delay may not be as desirable. Thus, the effects of Mach number and injector geometry were examined in these experiments as a means of evaluating the potential performance of lobed injector configurations for operation

Received 29 August 2001; revision received 15 April 2002; accepted for publication 18 November 2002.

*Graduate Student Researcher, Department of Mechanical and Aerospace Engineering; currently Member of the Technical Staff, The Aerospace Corporation, Los Angeles, CA 90009-2957.
†Professor, Department of Mechanical and Aerospace Engineering.
‡Professor, Department of Mechanical and Aerospace Engineering. Associate Fellow AIAA.

in a higher speed combustor context. The injectors analyzed in the present study included three alternative exit plane geometries: one square wave injector, one rounded square wave injector, and, for comparison, a nonlobed (or straight slot) injector.

Experimental Facility and Methods

The present experiments were conducted in the North American Trisonic (subsonic–transonic–supersonic) Wind Tunnel, owned by UCLA and operated by Allied Aerospace Industries, Inc., in El Segundo, California. The tunnel is capable of achieving flow conditions in its 2.13 m by 2.13 m test section ranging from Mach 0.1 to 3.5. In the present experiments, the Mach numbers of the bulk airflow ranged from 0.4 to 1.2 and the Reynolds number per meter ranged from 1.15×10^7 to 2.23×10^7. To achieve these conditions, the test section static pressures varied from 0.578 atm (corresponding to the highest Mach number) to 1.23 atm (corresponding to the lowest Mach number).

The entire apparatus used to perform these experiments, with the exception of the injectors themselves and the laser power supply, was housed inside a 2.23-m-long test fixture, which was 33.0 cm in height and 20.3 cm in width. This fixture was fitted with a leading-edge wedge that had a half-angle of 12 deg. Schematic diagrams of the interior views of the test fixture are shown in Fig. 2. The fixture was mounted on a tunnel sector head so that the fixture was situated in the center (in both the vertical and lateral directions) of the tunnel test section.

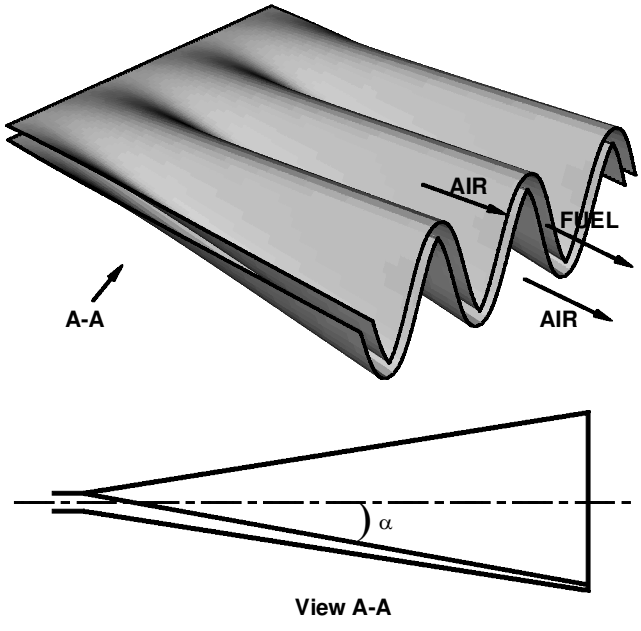

Fig. 1 Schematic of general lobed injector geometry.

In these nonreactive experiments, nitrogen was used as the fuel surrogate injected from the lobed injectors into the coflowing airstream, and acetone was used a tracer within the N_2 for quantification of mixing via acetone PLIF. The gaseous N_2 flowed from a high-pressure (276-atm) tank stored within the test fixture, as indicated in Fig. 2, through a solenoid valve (Marotta Model MV510H) used to start and stop the gas flow. The N_2 then flowed through a heated reservoir filled with liquid acetone and was controlled using an Omega model CN76000 autotune controller. After the acetone vaporized and mixed with the N_2, the mixture flowed through flexible tubing into the injector. The injector was situated outside of the test fixture, with the flat end positioned in the upstream direction and the corrugated end oriented toward the downstream, or positive z direction, as indicated in the lower part of Fig. 2. The injector was attached to the fixture with a mount that had an upstream leading edge wedge with a half-angle of 5 deg and side wedges with a half-angle of 9.9 deg.

Once the acetone exited the injector and encountered the high-speed coflowing air, the acetone within the nitrogen mixture was excited with a laser light sheet oriented perpendicularly to the direction of the bulk airflow (lower part of Fig. 2), in the x–y plane. The light source was a flashlamp-pumped, frequency quadrupled Nd:YAG laser (Lambda Physik, Model LPY-150) operating at a wavelength of 266 nm. The laser pulsed at 10 Hz with a pulse duration of 4 ns and energy of approximately 40 mJ per pulse. The UV laser light passed from the laser head (situated inside the test fixture), through a quartz window mounted on the side of the test fixture, into the evolving lobed injector flowfield. On excitation at 266 nm and decay from its excited state, the acetone emits fluorescence with an intensity proportional to its concentration.[21] Whereas the acetone concentrations in N_2 here were about 180,000 ppm, the average concentration of acetone downstream in the test section was well below 180,000 ppm, so that beam absorption was negligible. The laser light sheet was approximately 51 mm wide in the vicinity of the center of the lobed injector flowfield, with a sheet thickness of less than 500 μm.

An intensified charge-coupled device (CCD) camera (ITT Model F4577) situated within the fixture was used to capture this fluorescence, with optical access for the camera provided by a plexiglass window mounted in the fixture shown in the upper part of Fig. 2. Long-pass optical filters were placed in front of the imaging lens to prevent elastically scattered laser light from reaching the intensified CCD array. Imaging optics within the fixture allowed the camera to view the plane of the laser sheet as indicated in Fig. 2. Acetone phosphorescence (200-μs lifetime) was rejected by gating the image

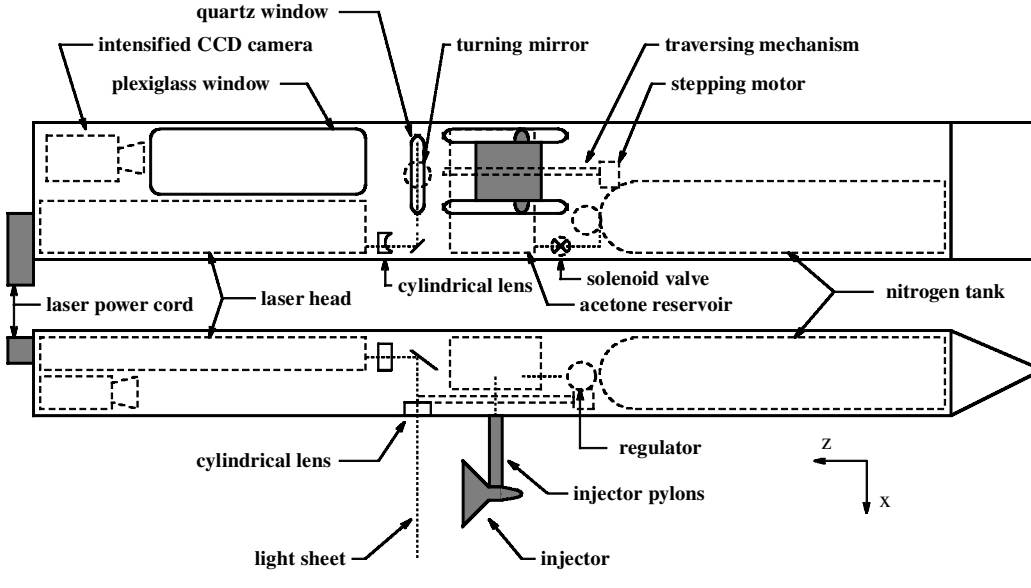

Fig. 2 Schematic of experimental test fixture: bottom, view of fixture interior seen from top of fixture, and top, interior as viewed from side of fixture.

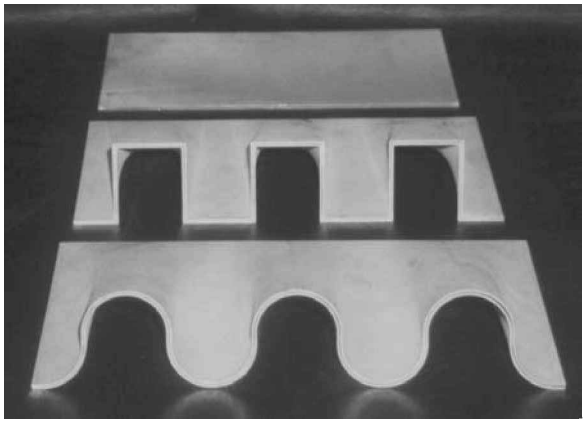

Fig. 3 Three injectors tested: bottom, injector A (rounded square wave); center, injector B (square wave); and top, injector C (straight slot).

intensifier on for a period of 200 ns. The imaging lens and CCD array combination gave a pixel resolution of better than 140 μm.

Each lobed injector under examination was mounted onto a traversing stage containing a lead screw driven by a stepping motor. Thus, when the injector was moved relative to the laser sheet, the evolution of the fuel concentration field was visualized at a range of downstream locations. The location of the injector, as it traversed relative to the laser sheet, was recorded with a linear position transducer (Space Age Control, Inc., Model 160), and its motion was controlled via a 12-bit acquisition and processing card (Tattletale Model 8). The distance between the injector and the fixture wall was 73 mm.

Three different injectors were used in this study. A photograph of the injectors is shown in Fig. 3. The two lobed injectors included one with a rounded square wave shape, labeled injector A, and one with a square wave shape, labeled injector B. The nonlobed or straight slot injector was labeled C. The nonlobed configuration was investigated in an attempt to isolate the effects of the lobes' near-field streamwise vorticity generation on the mixing characteristics of the injectors, as distinct from spanwise vorticity generation and small-scale turbulence. The lobed injector shapes, incorporating vertical or essentially vertical side walls, were designed on the basis of their potential for vorticity generation and rollup as predicted by an incompressible simulation of the flowfield.[2] Lobed mixers with vertical side walls are similarly observed to enhance streamwise vorticity generation.[5–9] All three injectors were fabricated of aluminum using an electrical discharge machining (EDM) device, and all three had the same injectant gap width (0.381 mm) and wall thickness (0.584 mm). Each lobed injector had a lobe angle α (Fig. 1) equal to 15 deg, a wavelength λ of 50.8 mm, and a peak-to-peak amplitude of 30.5 mm.

Visualization of the downstream evolution of injectant via acetone PLIF was made for fixed airflow Mach numbers of 0.4, 0.8, and 1.2 for each of the injectors. In each case, the video recording of the PLIF images began at one-eighth of a wavelength ($\frac{1}{8}\lambda$) downstream of the injector, to minimize reflections of the laser light at the injector exit plane, then the injector was moved at a constant velocity (5.1 mm/s, or 0.1 wavelength/s) away from the laser sheet. The injector traveled a distance of the order of two wavelengths in total. PLIF images were also recorded for cases where the distance between the injector exit and the laser sheet was fixed, at one-quarter wavelength downstream of the injector, while the bulk airflow Mach number in the tunnel was swept from about 0.8 to 1.1. In all experiments, the Mach number of the N_2 introduced between the injector plates was estimated to be approximately 0.2. This injection occurred over such a thin gap width (0.381 mm) that its contribution to spanwise vorticity generation was negligible as compared with the spanwise vorticity generation via the bulk high-speed flow above and below the injector. In all of the PLIF images, only the flowfield associated with the center lobe (or the center of the injector for the straight slot injector) was captured by the CCD camera to resolve mixing and scalar dissipation data more accurately.

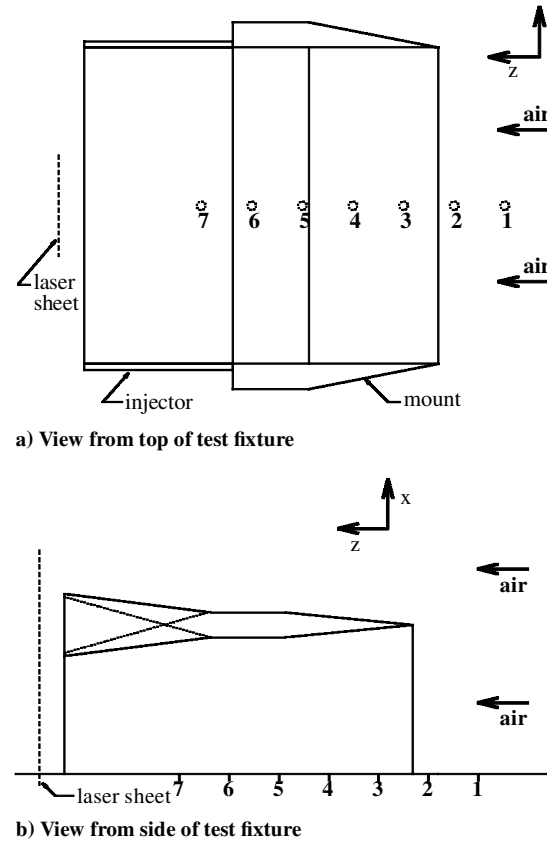

Fig. 4 Injector, mount, and locations of pressure transducers on test fixture skin.

Seven flush-mounted pressure transducers were placed along the test fixture side wall, beneath the center of the injector, to characterize the local flowfield under the injectors. The first transducer was located 76.2 mm upstream of the laser sheet and each of the six subsequent transducers was located farther upstream of the sheet in 25.4-mm increments. Schematics showing the top and side views of the locations of the pressure transducers relative to the injector and the laser sheet, for the "Mach sweep" runs, are given in Figs. 4a and 4b. The relative positions of the transducers correspond to the case where the tunnel Mach number was swept from 0.8 to 1.1 and the injector was fixed relative to the laser sheet and transducers. Figures 5a and 5b show the positions of these same transducers during the tests conducted at constant airflow Mach numbers, at the beginning (Fig. 5a) and the end (Fig. 5b) of the test runs, respectively. Hence, it was possible to obtain a relatively clear picture of the flow features beneath the injectors (on the fixture side) during each test run. The bulk airflow above each injector, on the opposite side of the fixture, was assumed to correspond to tunnel freestream conditions.

Quantification of Data

PLIF images of acetone fluorescence were converted to acetone concentration fields by dividing images by normalized calibration images. Pixel values in the scalar concentration images varied between 0 and 1, representing the mass fraction of N_2 at each pixel location. These PLIF images were then converted from N_2 mass fraction (Y) images to mixture fraction (ξ) images using the relation $\xi = Y/Y_f$, where Y_f is the maximum N_2 (fuel) mass fraction in the flowfield at injection. Pressure and temperature sensors within the acetone seeder allowed this quantification. Mixture fraction gradients ($\nabla\xi$) were calculated from pixel values of ξ using central differencing with a low-pass spatial filter. The scalar dissipation rate[22] χ was then calculated as $\chi = 2\mathcal{D}\nabla\xi \cdot \nabla\xi$, where $\mathcal{D}$ is the average mass diffusivity. In the present experiments, gradients were calculated along the interfacial regions between injectant and surroundings in two dimensions only. Although this evaluation clearly did not produce the complete value of scalar dissipation rate χ, it was reasoned that the component of χ arising from the streamwise

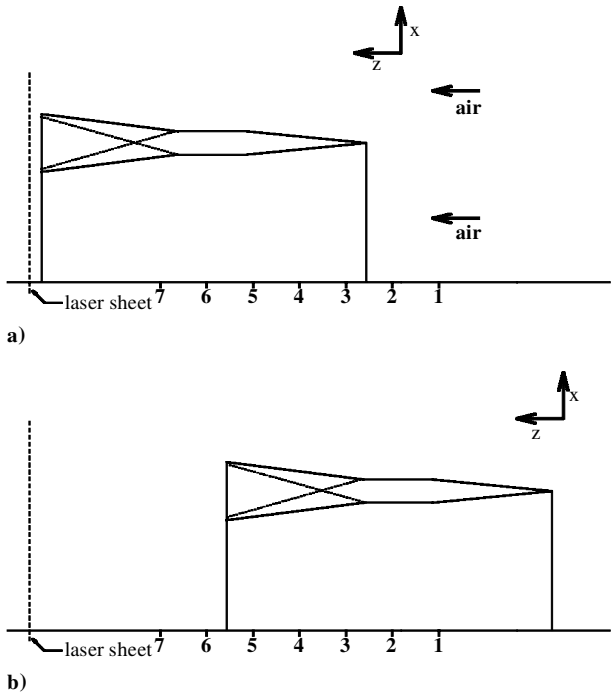

Fig. 5 View from side of test fixture; a) beginning of test run, laser sheet located at $z/\lambda = \frac{1}{8}$ beyond the injector exit, and b) end of test run, laser sheet located at $z/\lambda = 2\frac{1}{8}$ beyond the injector exit.

gradient in ξ should be roughly the same among the different injectors for the same flow conditions. Moreover, estimates of the gradients $\nabla\xi$ from image to image in the z direction were found to yield values much smaller than the gradients in the x–y planes. Hence, comparisons of χ among the different injectors, for the same flow conditions, should yield useful information with respect to the potential for interfacial straining. In the present experiments, local values of χ at stoichiometric interfaces ξ_{st}, that is, where $\nabla\xi$ or χ became locally maximum,[20] were averaged over half a lobe wavelength. These mean values of χ thus represented, at a given downstream location, a scaled measure of the effective strain field experienced at the injectant–air interfaces.

It is possible to relate the scalar dissipation rate χ to the strain rate ϵ at stoichiometric contours in an equivalent reactive flow, when one assumes that the interfaces between fuel and air behave as locally steady, opposed flow diffusion flames. This relationship between strain rate ϵ and scalar dissipation rate χ at a dissipation layer contour ξ_{st} is described in detail by Bish and Dahm[20] and is given by

$$\epsilon = \frac{\pi\chi}{(\xi_+ - \xi_-)^2} \cdot \exp\left(2\left\{\text{erf}^{-1}\left[\frac{\xi_{st} - \frac{1}{2}(\xi_+ + \xi_-)}{\frac{1}{2}(\xi_+ - \xi_-)}\right]\right\}^2\right) \quad (1)$$

As pointed out in previous work,[1] the values of the conserved scalar well above and below the mixing interface, ξ_+ and ξ_-, have a critical effect on the magnitude of the local strain rate experienced by the interface. In the present study, an automated technique was used[23] in which the dissipation layer contours ξ_{st} were determined by searching for local maxima in the scalar gradient field; it was at these locations that χ was computed. Then ξ_+ and ξ_- were estimated locally by a curve fit to the error function solution. This resulted in errors in ϵ that were limited to approximately 10–20% within one wavelength of the injector, but which could be more than 50% in the far-field region of the flowfield due to uncertainties in ξ_+ and ξ_- values. Hence, the results presented here will be limited to data taken within about one wavelength of the injector exit.

The degree of molecular mixing within a flowfield is quantified typically using the concept of mixedness[24] or the concept of unmixedness.[25] Both parameters quantify mixing in terms of the second moment of the scalar concentration field, which enables comparisons of the local scalar field to be made with the scalar field that would be present if the fluids were completely mixed (or completely unmixed). In the present analysis, the concept of unmixedness U was used to quantify molecular mixing processes. U is defined as follows:

$$U = \frac{\int_{Y_0}^{Y_1} (Y - \bar{Y})^2 \cdot p(Y)\,dY}{(Y_1 - \bar{Y})(\bar{Y} - Y_0)} \quad (2)$$

where Y_0 and Y_1 are the minimum and maximum N_2 mass fractions present within a given interrogation area, respectively, $p(Y)$ is the probability density function of the mass fraction, and the mean value of the mass fraction within the local interrogation area, $\bar{Y}$, is given by

$$\bar{Y} = \int_{Y_0}^{Y_1} Y \cdot p(Y)\,dY \quad (3)$$

Note that the unmixedness U approaches unity for the case of completely nonmolecularly mixed fluids, that is, the second moment in the numerator of Eq. (2) approaches the denominator. U approaches zero for complete molecular mixing of two fluids, that is, when the local mass fraction $Y = \bar{Y}$ everywhere within the integration region.

The degree of mixedness or unmixedness in a flowfield is sensitive to the integration area over which the second moment is evaluated, as pointed out by Marble.[24] As noted in previous experimental studies,[1] it is the local degree of fuel–air straining and mixing at stoichiometric interfaces that is relevant to ignition delay. As a consequence, in quantitatively comparing mixing characteristics among the injectors studied, we chose a rectangular integration area that included (at the injection plane) roughly one-half wavelength of a lobed injector, spanning from trough to peak. The initial N_2–air interface lengths, the cross-sectional areas of pure N_2 and pure air, and the total integration areas were fixed when computing mixedness values among the injectors investigated, including the straight injector. For the lobed injectors, the integration area always included the peak and inflection point of the injector flowfield. Hence comparisons of U among the three injectors yielded differences that arose mostly from secondary flows along the lobes and subsequent streamwise vorticity generation. The effects of different interfacial lengths of the injectors were, thus, removed from the computation of unmixedness. Also as done in previous experiments,[1] the integration area and location for the evaluation of unmixedness were maintained as constants for a given injector as downstream location was varied.

Results

Sample PLIF images showing the flow evolution for the square wave injector B at an airflow Mach number of 0.4 are given in Fig. 6, with images shown at different locations z downstream of the injector exit plane scaled with respect to the injector wavelength λ. As already noted, N_2 injection over the very thin injector gap widths was essentially fixed at Mach 0.2 (approximately 70 m/s) for all cases examined. Evolution within one wavelength of the injection plane was clearly visible in these PLIF images and was also visible for Mach 0.8 airflow conditions (Fig. 7). Beyond 1.5 wavelengths, and for Mach 1.2 airflow conditions, acetone PLIF images were often too washed out to obtain accurate quantitative data. So that the injectant is more clearly visible, fluorescence intensity rather than mass fraction is shown in all PLIF images. Evidence of streamwise rollup of vortical structures was observed in Fig. 6, particularly in the vicinity of the injector corners. This rollup appeared to strain out the injectant in the region of these corners, as indicated by the reduction in PLIF signal. The flow evolution from the square wave injector was such that the square wave shape was not retained downstream, but rather was skewed into a series of alternating "keyhole" shapes within one wavelength.

When the Mach number of the coflowing air was increased to 0.8 for square wave injector B, with the injectant Mach number fixed at 0.2, the vortex rollup and injectant distortion processes accelerated somewhat, as indicated in Fig. 7. A more obvious trend, however, was the much more rapid mixing out of the injectant at a given downstream distance due to the higher speed coflow. (The signal

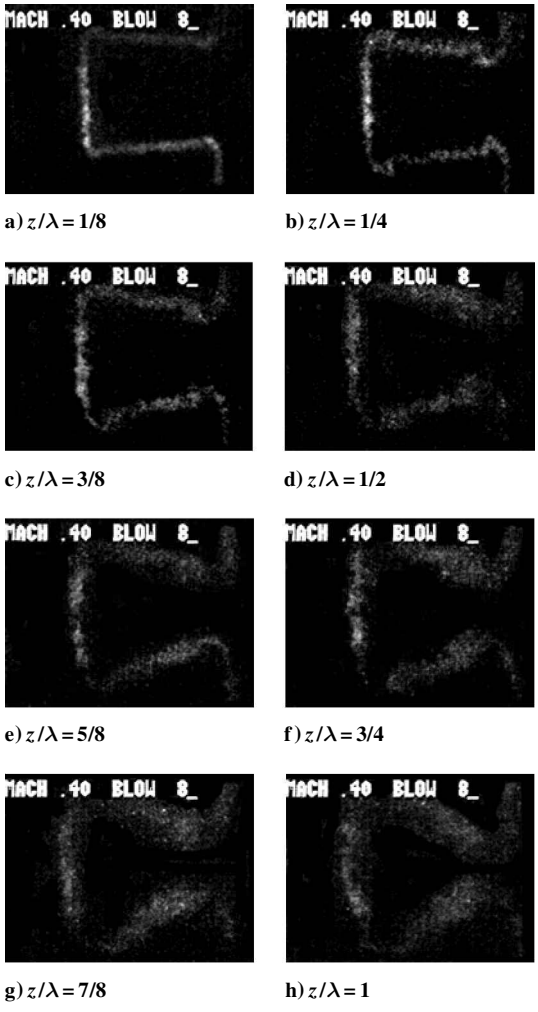

a) $z/\lambda = 1/8$ b) $z/\lambda = 1/4$

c) $z/\lambda = 3/8$ d) $z/\lambda = 1/2$

e) $z/\lambda = 5/8$ f) $z/\lambda = 3/4$

g) $z/\lambda = 7/8$ h) $z/\lambda = 1$

Fig. 6 PLIF images of N_2 mass fraction; evolution of center lobe region of square wave injector B, for Mach 0.4 tests.

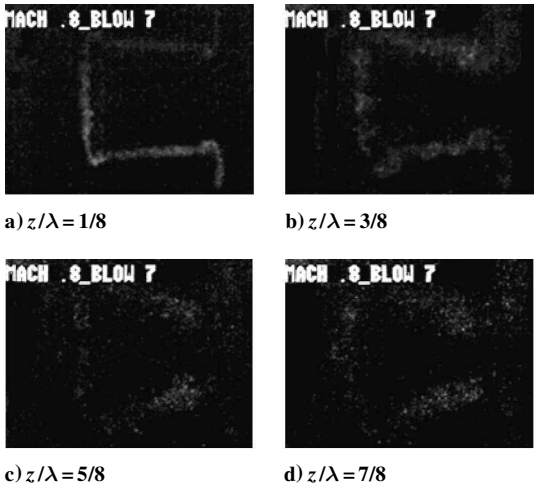

a) $z/\lambda = 1/8$ b) $z/\lambda = 3/8$

c) $z/\lambda = 5/8$ d) $z/\lambda = 7/8$

Fig. 7 PLIF images of N_2 mass fraction; evolution of center lobe region of square wave injector B, for Mach 0.8 tests.

gain was the same for all PLIF images shown in Figs. 6 and 7.) Once again, for the square wave injector, the evolving flow distorted into the series of alternating keyhole shapes. When the rounded square wave injector, injector A, was used, this type of distortion into a keyholelike shape was also observed, as indicated in Fig. 8. For comparison, the evolution of flow from the straight slot injector C is shown in Fig. 9. Figure 9 shows images at different locations z downstream of the straight injector exit plane scaled with respect to the wavelength of the lobed injectors (50.8 mm). Only small-scale turbulent mixing was observed to affect the slot injector flowfield in its downstream evolution; no significant streamwise vorticity caused any larger-scale flow distortion.

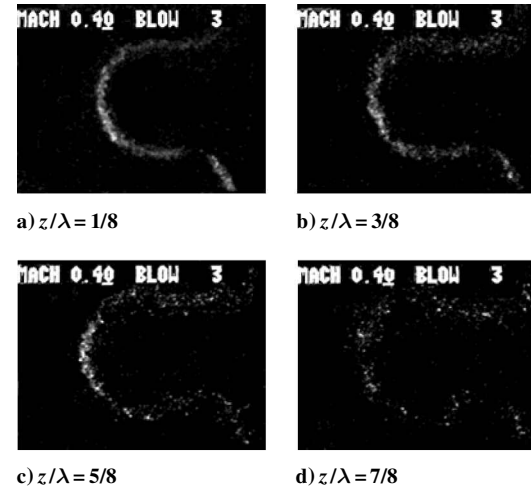

a) $z/\lambda = 1/8$ b) $z/\lambda = 3/8$

c) $z/\lambda = 5/8$ d) $z/\lambda = 7/8$

Fig. 8 PLIF images of N_2 mass fraction; evolution of center lobe region of rounded square wave injector A, for Mach 0.4 tests.

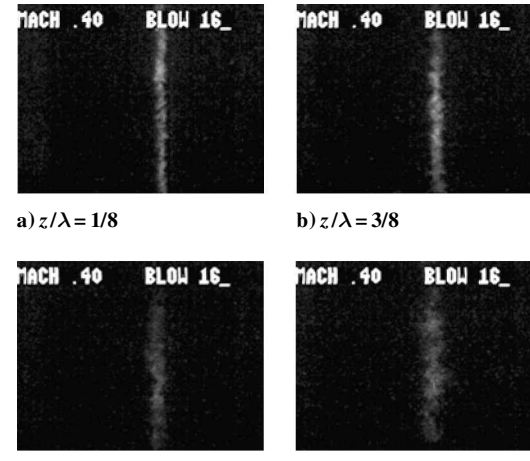

a) $z/\lambda = 1/8$ b) $z/\lambda = 3/8$

a) $z/\lambda = 5/8$ b) $z/\lambda = 7/8$

Fig. 9 PLIF images of N_2 mass fraction, evolution of center region of straight slot injector C, for Mach 0.4 tests.

Although it might be surmised that the distortion of the flowfield from the lobed injectors arose from the effect of the oppositely oriented secondary flows along the injector side walls, the distortion actually arose due to small errors in injector fabrication by the EDM process. Whereas the ideal injector should be cut by an EDM wire that is always perfectly aligned with the axial z direction, the actual cutting process for fabrication of the injectors occasionally skewed the wire so that it did not remain parallel to z as the lobed shape was cut.

The effect of this skewing on the flow evolution was determined by making a comparison of experimental observations such as those in Fig. 6 with numerical simulations of the lobed injector flowfield, using the vortex element method previously used and described in detail by Strickland et al.[2] Details on the present simulation may be found in Ref. 26. The simulation incorporated an array of viscous vortex blobs at the exit plane of the injector to represent the shape of the injector. Boundary conditions were incorporated in which the flow component normal to the injector surface was set to zero, which resulted in a solution for the distribution of vortex element strengths at the injector exit plane that was dependent on injector geometry. This distribution, thus, reflected the vorticity generation that occurred due to the spatial growth of lobed shape, from a flat shape at the upstream end to the corrugated shape at the exit plane. There were 668 vortex blobs per injector wavelength used in this simulation. The finite length of the injector in the y direction (due to the absence of full side walls adjacent to the injector) was represented in the model; this constituted a significant departure from the "infinite"

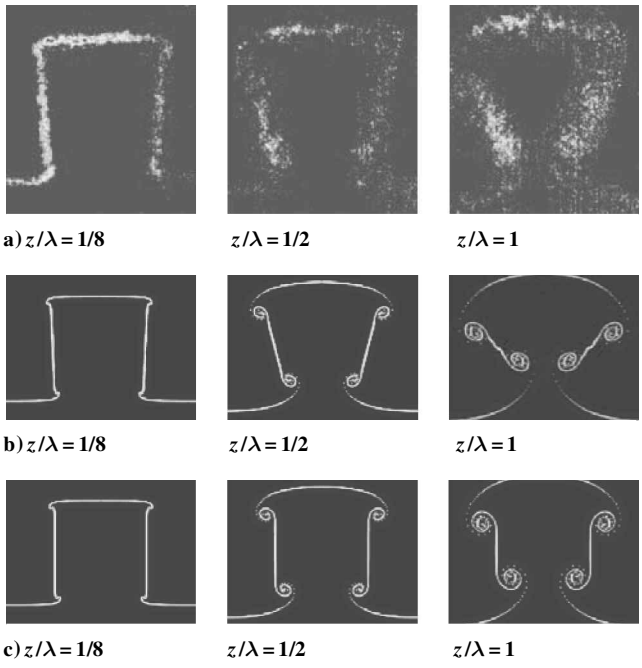

Fig. 10 Injectant from square wave lobed injector B, at different downstream locations, as determined from a) acetone PLIF experiments with actual lobed injector shape, b) computations of the flow or vorticity distribution with actual lobed injector shape as input, and c) computations the flow or vorticity distribution with lobed injector shape that would be formed by an ideal EDM wire cut.

injector configurations studied previously.[2] The present simulation was conducted under incompressible conditions, for comparison with the present low subsonic flow cases (Mach 0.4). Although this comparison is imperfect, note that an essentially incompressible vortex model for the lobed mixer[27] was able to replicate quite well the flow evolution for compressible lobed mixers. Tew[27] found that this replication held even for convective Mach numbers $M_c \equiv \frac{1}{2}(M_{\text{upper}} - M_{\text{lower}})$, based on the difference between the upper and lower bulk Mach numbers, as high as 0.56.

In the computations performed, the actual shape or growth of the lobed injector, as cut by the EDM wire, was used as one set of input boundary conditions for the determination of the vorticity distribution at the exit plane of the injector. This distribution of vorticity and its downstream evolution were compared with the ideal distribution of vorticity at the exit plane that would arise if the EDM wire had cut the injector perfectly, that is, with the wire continually lying parallel to the z axis during the cut. The results of this simulation are shown in Fig. 10; comparison of the actual experimental flow evolution was made with the computed evolution for both the ideal and the actual injector flowfield. When the exit plane vorticity arising from the actual wire cut was used in the simulation, the skewing of the flow into the keyhole shape observed in the experiments was replicated. When the ideally cut injector was represented numerically, this skewing did not appear, and only the vorticity rollup at the corners of the square shape became prominent. Hence, even relatively minor alterations in the nature of the growth of the lobed shapes were observed to affect flow evolution in a significant way.

As noted in Figs. 6 and 7, the injectant was mixed out more rapidly at higher coflow Mach numbers. The effects of Mach number on the flowfield are seen more extensively in the images in Fig. 11, where the flowfield at an axial location $z/\lambda = 0.25$ is shown for Mach numbers ranging from 0.825 to 1.1. Whereas the mixing appeared visually to increase overall between Mach 0.825 and 1.1, there appeared to be somewhat less mixing (and, hence, a higher concentration of reactant) during the sonic transition. This trend was found for other injectors, not only for the square wave injector B. The quantification of this observation is described later, in terms of the unmixedness parameter.

PLIF images such as those shown in Figs. 6–11 were used to quantify mixing and interfacial straining via the unmixedness, scalar

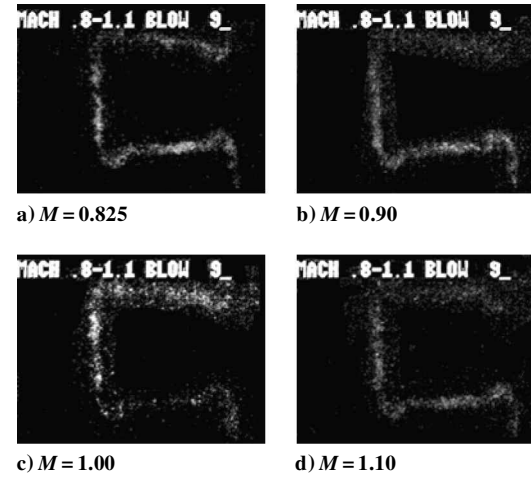

Fig. 11 PLIF images of N_2 mass fraction; center region of the square wave injector B at an axial location $z/\lambda = 0.25$, for four coflow Mach numbers, with injectant Mach number fixed at 0.2.

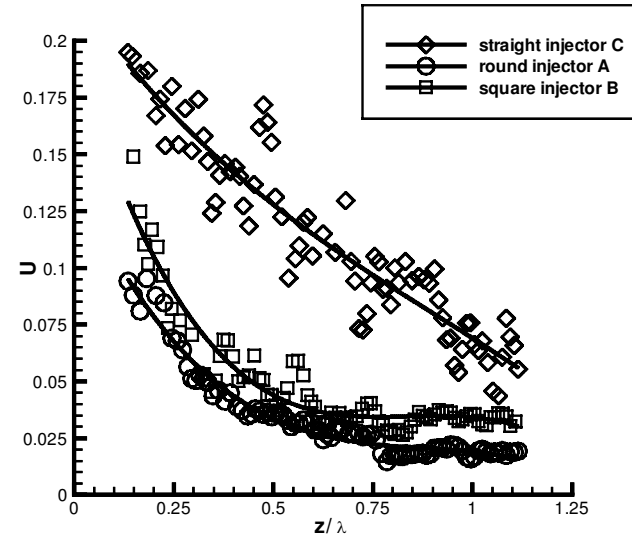

Fig. 12 Local unmixedness U as a function of normalized downstream distance z/λ for Mach 0.4 coflowing air; injectors A, B, and C compared.

dissipation rate, and average strain rate parameters. Comparisons of unmixedness among the three injectors for the Mach 0.4 case are shown in Fig. 12. Note that the value of U in this and subsequent quantifications of U, χ, and ϵ is a running average value, which takes into account three successive PLIF images to help compensate for possible shot-to-shot energy fluctuations in the laser sheet. Clearly, both lobed injector configurations were able to mix the injectant and coflowing air to a greater extent, from the beginning, than the equivalent straight injector. Because interfacial lengths were kept constant in the interrogation area for this comparison, the differences here arose principally due to the secondary flows initiated by the lobed shapes, creating local shear zones and vortical structures in the x–y plane to promote mixing. The spatial decay of unmixedness (or increase in mixing) for the lobed injectors also was greater than for the nonlobed injector, which further indicated the benefit of the lobed shape for mixing enhancement. The differences in unmixedness measured between the two lobed injectors (A and B) were small, nearly within the uncertainty in the measurement of the U value (± 0.005). When the Mach number of the coflowing air was increased to 0.8, the unmixedness for a given injector was observed to drop (Fig. 13), consistent with the corresponding PLIF images. The rate of decay in U was essentially the same between the two Mach numbers, however, for a given injector.

When the position of a given injector was fixed relative to the laser sheet, and the airflow Mach number swept between 0.8 and 1.1, interesting phenomena were quantified with respect to mixing,

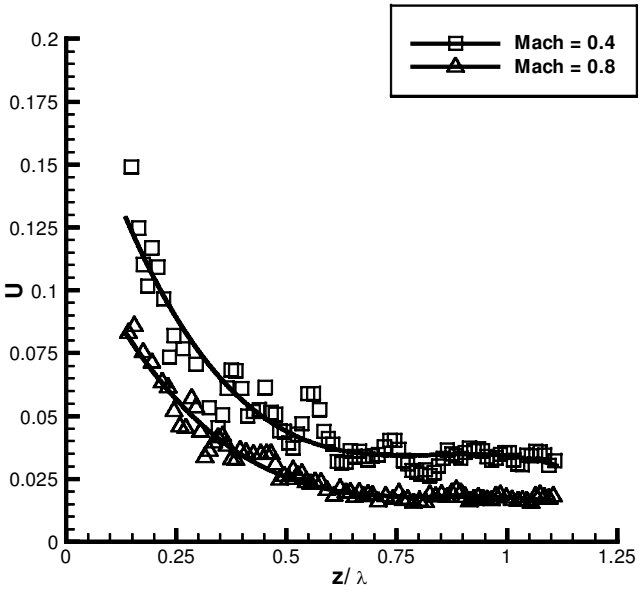

Fig. 13 Local unmixedness U as a function of normalized downstream distance z/λ for the square wave injector B; Mach 0.4 and 0.8 coflowing air compared.

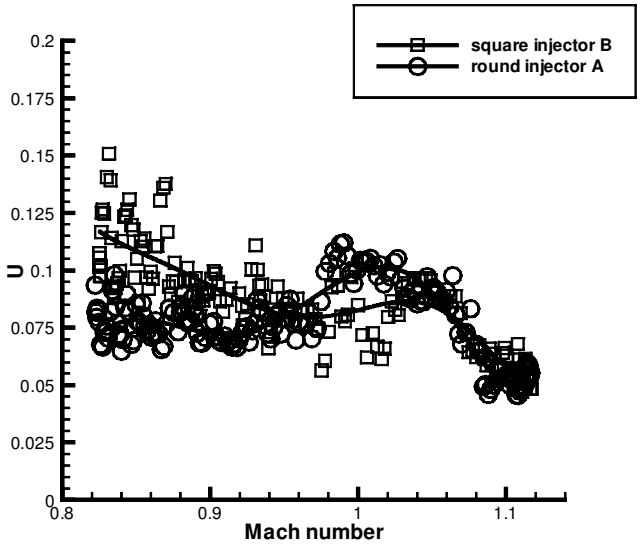

Fig. 14 Local unmixedness U as a function of coflowing air Mach number, at downstream location $z/\lambda = 0.25$; lobed injectors A and B compared.

as indicated in Fig. 14. An overall decay in unmixedness between Mach 0.8 and 1.1 was expected, but in all injectors examined, there appeared to be a slight increase and then a decay in U as the flow speed increased through Mach 1.0. These observations may be explained from data provided from the pressure transducers.

The pressure transducers provided evidence for the nature of the flow in the vicinity of the injector exit plane. As indicated in Figs. 5a and 5b, when the Mach number was fixed in the present test runs, the injector was moved relative to the laser sheet and to the fixed pressure transducers. Data from the pressure transducers in these test runs thus provided information regarding the spatial variation in pressure along the fixture, under the injectors. The pressure distribution was then converted to a distribution in Mach number, when the stagnation pressure of the gas about and in the vicinity of the injector was assumed to be constant for these runs. Even at a freestream Mach number of 1.2, this assumption of constant stagnation pressure was estimated to be good to at least 0.72% (when in the worst case, the presence of a bow shock upstream of the fixture or injector was assumed).

The results for the computed spatial variation in local Mach number for the flow under the injector, measured as a function of a negative distance "upstream" of the injector exit, are shown in Figs. 15a–15c, for freestream Mach numbers of 0.4, 0.8, and 1.2, respectively. The leading-edge of the injector mount was located at $z/\lambda = -3.5$. The results here correspond to data taken for the rounded square wave injector A, but very similar results were obtained for the other injectors. These data indicated that, for subsonic freestream conditions, the flow between the injector and the fixture tended to accelerate then decelerate from the upstream to the downstream (exit) portion of the injector, exiting at roughly the same Mach number as for the freestream, M_0 (Figs. 15a and 15b). Hence, in this subsonic regime, the flow below the injector appeared to behave as a subsonic nozzle, although at the exit plane there appeared to be a little mismatch between the Mach numbers of the flows above and below the injector. For the case of a freestream Mach number of 1.2 (Fig. 15c), the flow ahead of the injector (in the regime $z/\lambda < -3.5$) appeared to have been decelerated ahead of the injector to subsonic conditions, possibly due to shock structures upstream of the injector. The flow then accelerated as it continued from upstream to downstream beneath the injector, but again, exited at a Mach number of approximately the freestream value $M \approx 1.2$. In this slightly supersonic regime, the flow under the injector appeared to behave somewhat like a Laval nozzle, with an acceleration through sonic flow and an exit at supersonic conditions.

Greater evidence for the changing flow character about the lobed injectors in this transonic regime is provided from static pressure measurements made during the Mach sweep in which the injector was fixed at a location one-quarter of a wavelength upstream of the laser sheet and, hence, was also fixed with respect to the pressure transducers. Figure 16 shows, for different freestream Mach numbers ranging from 0.85 to 1.1, the static pressure measurements made by transducers 1–7, situated as shown relative to the injector in Fig. 4. The upstream edge of the injector was situated between transducers 2 and 3. The corresponding static pressure of the freestream is also shown. Interestingly, the differences between the static pressure at 7 (the point closest to the exit plane) and the freestream static pressure were rather small for Mach numbers near 0.825 and 1.1, but these differences increased as the freestream Mach number M_0 approached the transonic regime (that is, for M_0 between 0.90 and about 1.0). Because the gap width and wall thicknesses of the injectors were so small (0.381 and 0.584 mm, respectively), the Mach 0.2 injectant is viewed to have played a minor role in this upper–lower stream bulk pressure and velocity mismatch.

In fact, if one plots the difference between the Mach number at transducer 7 and the freestream Mach number, as indicated in Fig. 17, a peak in this Mach number difference $(M_7 - M_0)$ was observed at a freestream Mach number of about 0.94. This Mach number difference is not precisely linearly related to the actual convective Mach number because the speeds of sound above and below the injector may not be identical; however, the behavior of the $(M_7 - M_0)$ parameter does suggest that the behavior of the flow between the injector and the fixture materially changed character as the flow approached and underwent sonic conditions. That the Mach number difference in Fig. 17 was a maximum at a freestream Mach number of 0.94 may suggest that, due to nonlinear effects, the actual convective Mach number at the injector exit (in the shear layer between the streamwise flow above and below the injector) may have been relatively large. The experiments of both Papamoschou and Roshko[15] and Urban and Mungal[16] for turbulent compressible shear flows suggest that, for convective Mach numbers above about 0.25, the layer thickness and mixing as well as turbulent shear stresses start to diminish. There also exists some evidence, observed by Hall et al.,[28] that, even for convective Mach numbers as low as 0.1, there can be a sizable reduction in the compressible shear layer growth rate. Thus, it is likely, although not conclusively proven here, that, as the freestream Mach number encountered the sonic regime in the present experiments, the actual convective Mach number at the trailing edge of the injector became maximized and, hence, caused a reduction in the spanwise mixing characteristics of the flowfield. This could explain the local increase then decrease in unmixedness in the range of Mach 0.95–1.05 observed in Fig. 14.

Although the differences among the abilities of different lobed injectors to enhance mixing were clear when examining the unmixedness quantity, they became less obvious when examining

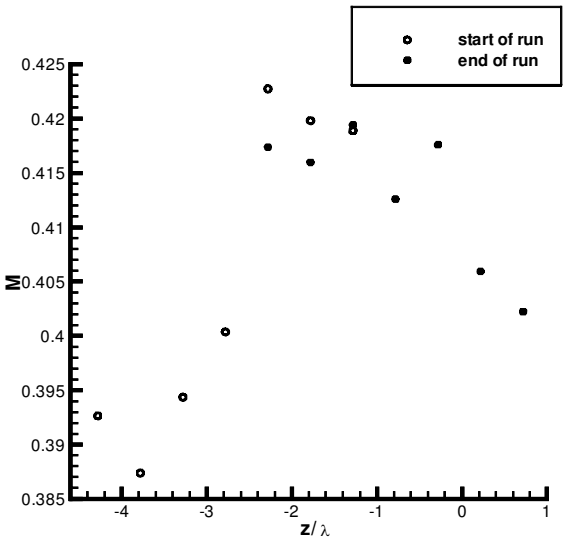

a) $M_0 = 0.4$

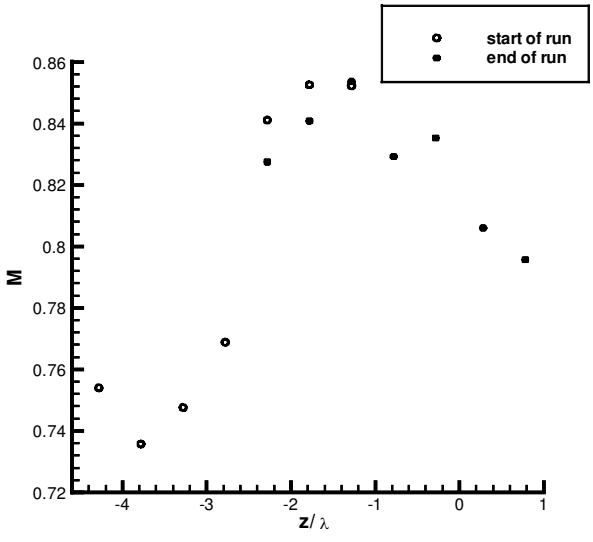

b) $M_0 = 0.8$

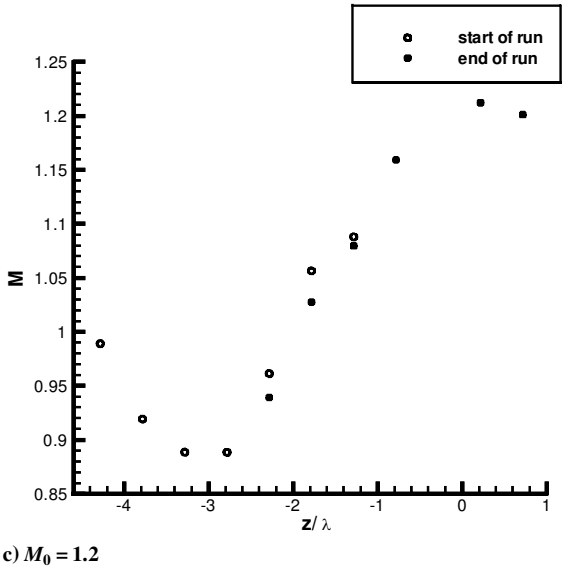

c) $M_0 = 1.2$

Fig. 15 Variation in local Mach number (computed from local static pressure) along the fixture, under lobed injector A, with respect to distance measured upstream of the exit plane of the injector ($z/\lambda = 0.0$): ○, start of the run, that is, injector $\frac{1}{8}\lambda$ upstream of laser sheet; and ●, end of the run, that is, injector $2\frac{1}{8}\lambda$ upstream of laser sheet.

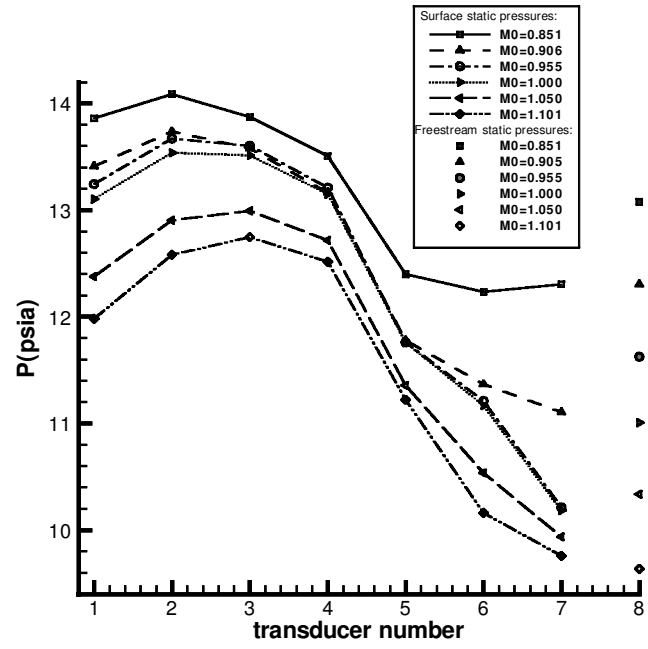

Fig. 16 Static pressure measurements of transducers 1–7, situated as shown relative to injector A in Fig. 4, for $M_0 = 0.85$–1.1, during a Mach number sweep; corresponding static pressures of the freestream are indicated as filled symbols, collectively called transducer 8.

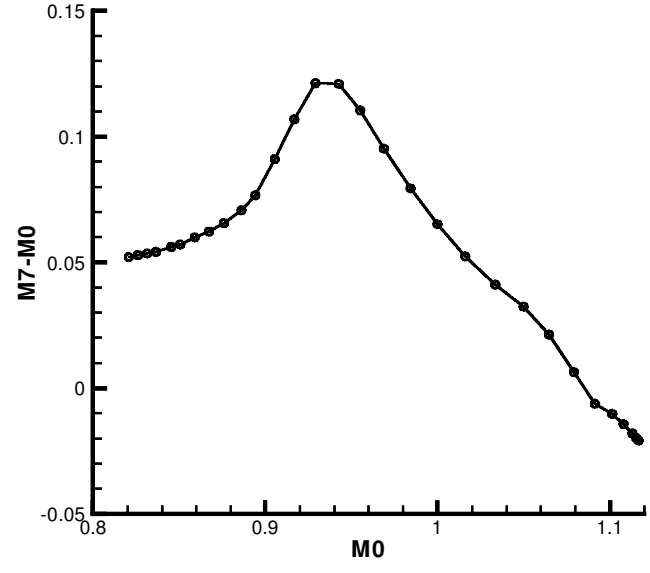

Fig. 17 Difference between the Mach number at transducer 7, M_7, (computed from the measured static pressure) and the freestream Mach number, M_0, as a function of freestream Mach number for data taken during a Mach sweep between 0.8 and 1.1.

mean scalar dissipation rate. Figure 18, for example, plots the mean value of the scalar dissipation rate χ along the ξ_{st} contours for different injectors as a function of downstream distance. Despite the fact that the lobed injectors, particularly square wave injector B, created greater vorticity in the near field, which is normally associated with increased strain, no significant differences in scalar dissipation rate were detected between lobed and nonlobed injectors. Nevertheless, as indicated in Eq. (1), the relation between the actual strain rate ϵ and the scalar dissipation rate χ is strongly dependent on the values of the conserved scalar, ξ_+ and ξ_-, well above and below the mixing interface, respectively. In the present problem, these values were influenced by the level of mixing of the injectant. Hence, extraction of the average strain rate along the stoichiometric contours provides a more useful comparison among the injectors tested.

Figure 19 shows the average strain rate ϵ along the contours of maximum χ for all three injectors, at a lower subsonic freestream Mach number (0.4) and plotted as a function of the normalized

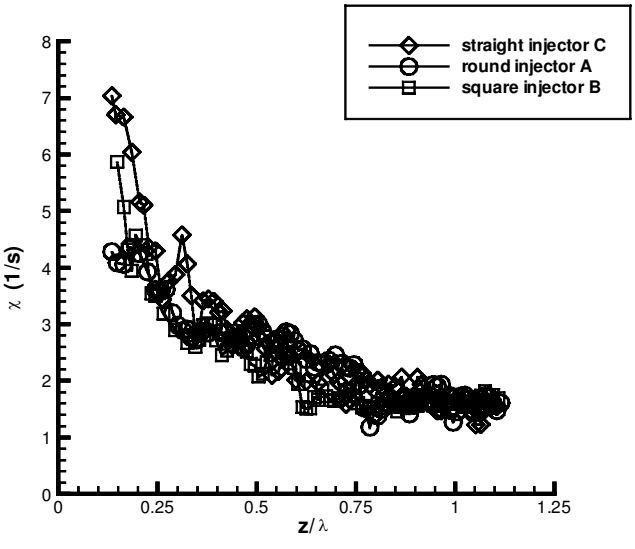

Fig. 18 Mean value of scalar dissipation rate χ along the contours of maximum χ, as a function of scaled downstream distance z/λ, for Mach 0.4 airflow; injectors A, B, and C compared.

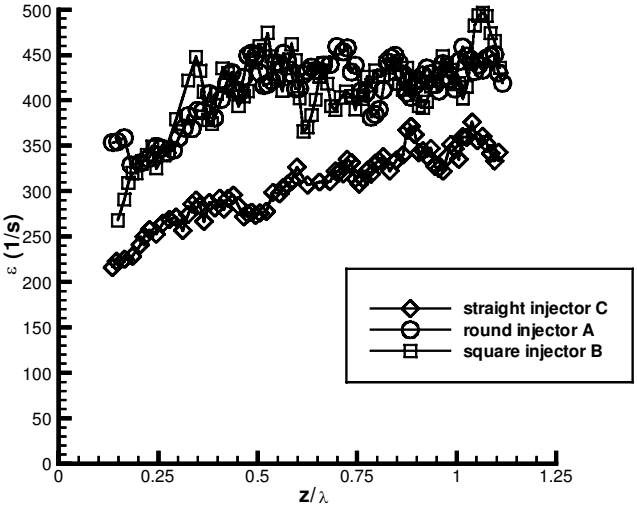

Fig. 19 Mean value of strain rate ϵ along the contours of maximum χ, as a function of scaled downstream distance z/λ, for Mach 0.4 airflow; injectors A, B, and C compared.

downstream distance z/λ. As in Figs. 12–14 and 18, the values indicated are a running average of computations from three successive PLIF images. Despite all three injectors' having relatively similar scalar dissipation rates (see Fig. 18), both lobed injectors A and B produced higher strain rates than the straight slot injector C, in some locations higher by as much as 50%. Strain rates for both lobed injectors asymptoted to about the same value of 430 s^{-1}, whereas the straight slot injector took longer to reach its asymptotic value of approximately $\epsilon = 340$ s^{-1}. These values compare with a critical strain rate for ignition delay of a propane fuel strip[29] of around 400 s^{-1}. Because of the higher strain rates associated with both lobed injectors in comparison to the straight slot injector, it can be deduced that the secondary velocities due to the lobed geometries in subsonic flow may in fact have added a significant rate of strain to the injectant, potentially enough to delay ignition when using the lobed injector in a low subsonic reacting flowfield.

The effect of compressibility on average strain rates yielded somewhat surprising results, that is, when compared with the improvement in mixing seen at Mach 0.8 in Fig. 13. When calculating the average strain rate for square wave injector B at the higher freestream Mach number of 0.8, it was found that the strain rate was actually reduced slightly as compared to the Mach 0.4 case (Fig. 20). This result was consistent with corresponding scalar dissipation rate results for Mach 0.8. Hence, although mixing increased for the lobed injector between Mach 0.4 and 0.8, the effective strain rate was observed to drop. The behavior of the lobed injector's strain field at higher subsonic speeds may actually suggest an added benefit of the device. In transonic and supersonic combustors, it is desired to mix and burn reactants rapidly, to allow completion of the reaction process within a relatively short combustor length. The limited results here suggest that at Mach 0.8, higher mixing (Fig. 13) and the greater potential for ignition (Fig. 20) may simultaneously be possible with the lobed injector configuration.

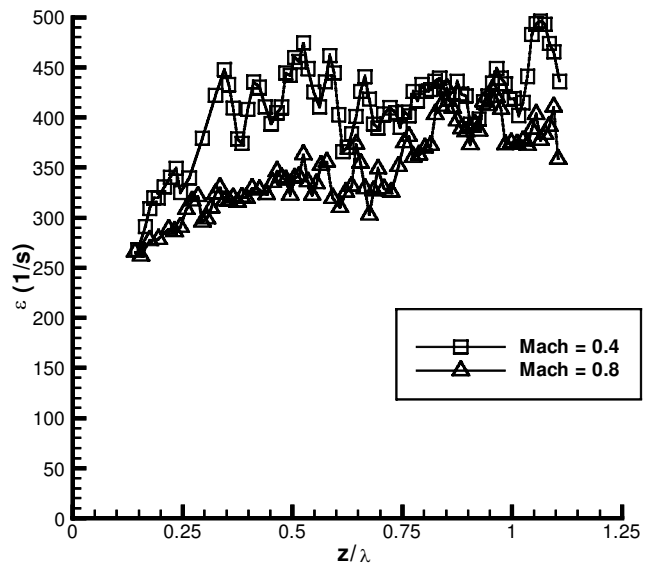

Fig. 20 Mean value of strain rate ϵ along the contours of maximum χ, as a function of scaled downstream distance z/λ, for the square wave injector B; Mach 0.4 and 0.8 coflowing air compared.

Conclusions

Through high-speed wind tunnel experiments on several injector geometries, lobed shapes were quantified in the near field to mix injectant more rapidly and to a greater extent than nonlobed (or straight slot) fuel injectors. Increases in coflow Mach number, from 0.4 to 0.8, resulted in increased magnitudes of secondary velocities, as well as increased streamwise shearing. Thus, mixing was found to increase as well. Distortion in the spatial growth of the injector itself, due to skewing of the EDM wire during fabrication, was found to create significant differences in flow evolution. Based on the required vorticity rollup and mixing enhancement, this skewing may in fact be desirable in some combustion applications.

In the near field, scalar dissipation rates were not observed to be significantly different between lobed and nonlobed injectors, but when corresponding strain rates were extracted, lobed injectors were found to exhibit higher average strain rates than did the nonlobed straight injector, by as much as 50% at Mach 0.4. At Mach 0.8 conditions, however, while mixing increased, interfacial strain rates dropped when compared with Mach 0.4 conditions, suggesting that both enhanced mixing and high-speed ignition were possible using this injector at higher speeds. This may in fact have benefits for operation of the lobed injector well into the transonic/supersonic regime.

Acknowledgments

The research reported here was supported by NASA Dryden Flight Research Center under Grant NCC-2-374 (S. Corda and K. Iliff, Grant Monitors) and by the Former Dean of the Henry Samueli School of Engineering and Applied Science at the University of California, Los Angeles (UCLA), A. R. Frank Wazzan. The authors acknowledge the assistance of Robert Lobbia, Lydia Trevino, and Jonathan King of UCLA; Rick Hughes and the technical staff at Allied Aerospace Industries, Inc.; the technical staffs at Big Sky Laser and Lambda Physik; and Frank E. Marble of the California Institute of Technology in various phases of this study.

Helpful comments by Iskender Gokalp of the Centre National de la Recherche Scientifique, Orleans, France, are also acknowledged with gratitude.

References

[1]Smith, L. L., Majamaki, A. J., Lam, I. T., Delabroy, O., Karagozian, A. R., Marble, F. E., and Smith, O. I., "Mixing Enhancement in a Lobed Injector," *Physics of Fluids*, Vol. 9, No. 3, 1997, pp. 667–678.

[2]Strickland, J. H., Selerland, T., and Karagozian, A. R., "Numerical Simulations of a Lobed Fuel Injector," *Physics of Fluids*, Vol. 10, No. 11, 1998, pp. 2950–2964.

[3]Mitchell, M. G., Smith, L. L., Karagozian, A. R., and Smith, O. I., "Burner Emissions Associated with Lobed and Non-Lobed Fuel Injectors," *Twenty-Seventh Symposium (International) on Combustion*, Combustion Inst., Pittsburgh, PA, 1998, pp. 1825–1831.

[4]Mitchell, M. G., Smith, O. I., and Karagozian, A. R., "Effects of Passive Fuel–Air Mixing Control on Burner Emissions via Lobed Fuel Injectors," AIAA Paper 99-2400, June 1999.

[5]O'Sullivan, M. N., Krasnodebski, J. K., Waitz, I. A., Greitzer, E. M., and Tan, C. S., "Computational Study of Viscous Effects on Lobed Mixer Flow Features and Performance," *Journal of Propulsion and Power*, Vol. 12, No. 3, 1996, pp. 449–456.

[6]Presz, W. M., Morin, B. L., and Gousy, R. G., "Forced Mixer Lobes in Ejector Designs," *Journal of Propulsion and Power*, Vol. 4, No. 4, 1988, pp. 350–355.

[7]Eckerle, W. A., Sheibani, H., and Awad, J., "Experimental Measurements of Vortex Development Downstream of a Lobed Forced Mixer," *Journal of Engineering for Gas Turbines and Power*, Vol. 114, No. 1, 1992, pp. 63–71.

[8]Skebe, S. A., Paterson, R. W., and Barber, T. J., "Experimental Investigation of Three-Dimensional Forced Mixer Lobe Flow Fields," AIAA Paper 88-3785-CP, 1988.

[9]Tew, D. E., Teeple, B. S., and Waitz, I. A., "Mixer-Ejector Noise-Suppressor Model," *Journal of Propulsion and Power*, Vol. 14, No. 6, 1998, pp. 941–950.

[10]McVey, J. B., "Observation of the Effect of Streamwise Vorticity on the Spreading of Flames in High Speed Flow," *Combustion Science and Technology*, Vol. 60, No. 1–6, 1988, pp. 447–451.

[11]McVey, J. B., and Kennedy, J. B., "Flame Propagation Enhancement Through Streamwise Vorticity Stirring," AIAA Paper 89-0619, 1989.

[12]Waitz, I. A., and Underwood, D. S., "Effect of Heat Release on Streamwise Vorticity Enhanced Mixing," *Journal of Propulsion and Power*, Vol. 12, No. 4, 1995, pp. 638–645.

[13]Tillman, T. G., Patrick, W. P., and Paterson, R. W., "Enhanced Mixing of Supersonic Jets," *Journal of Propulsion and Power*, Vol. 7, No. 6, 1991, pp. 1006–1014.

[14]Tillman, T. G., Paterson, R. W., and Presz, W. M., "Supersonic Nozzle Mixer Ejector," *Journal of Propulsion and Power*, Vol. 8, No. 2, 1992, pp. 513–519.

[15]Papamoschou, D., and Roshko, A., "The Turbulent Compressible Shear Layer: An Experimental Study," *Journal of Fluid Mechanics*, Vol. 197, 1988, pp. 453–477.

[16]Urban, W. D., and Mungal, M. G., "Planar Velocity Measurements in Compressible Mixing Layers," *Journal of Fluid Mechanics*, Vol. 431, 2001, pp. 189–222.

[17]Srikrishnan, A. R., Kurian, J., and Sriramulu, V., "Enhancement of Thermal Mixing in Coaxial Supersonic Jets," *Journal of Propulsion and Power*, Vol. 12, No. 1, 1996, pp. 165–169.

[18]Kumar, R. R., and Kurian, J., "Estimation of Mixing of High-Speed Streams," *Journal of Propulsion and Power*, Vol. 12, No. 2, 1996, pp. 429–431.

[19]Rajamanohar, D., and Kurian, J., "Preliminary Studies on Dual-Mode Combustion Ramjet Using Petal Nozzle," *Journal of Propulsion and Power*, Vol. 12, No. 2, 1996, pp. 424–426.

[20]Bish, E. S., and Dahm, W. J. A., "Strained Dissipation and Reaction Layer Analyses of Nonequilibrium Chemistry in Turbulent Reacting Flows," *Combustion and Flame*, Vol. 100, No. 3, 1994, pp. 457–466.

[21]Lozano, A., Yip, B., and Hanson, R. K., "Acetone: A Tracer for Concentration Measurements on Gaseous Flows by Planar Laser-Induced Fluorescence," *Experiments in Fluids*, Vol. 13, 1992, pp. 369–376.

[22]Peters, N., "Local Quenching Due to Flame Stretch and Non-Premixed Turbulent Combustion," *Combustion Science and Technology*, Vol. 30, 1983, pp. 1–17.

[23]Lam, I., "A Computational Procedure for the Interrogation of Mixing and Reacting Layers," M.S. Thesis, Dept. of Mechanical and Aerospace Engineering, Univ. of California, Los Angeles, 1996.

[24]Marble, F. E., "Mixing, Diffusion, and Chemical Reaction of Liquids in a Vortex Field," *Chemical Reactivity in Liquids*, edited by M. Moreau and P. Turq, 1987, pp. 581–596.

[25]Dimotakis, P. E., and Miller, P. L., "Some Consequences of the Boundedness of Scalar Fluctuations," *Physics of Fluids A*, Vol. 2, No. 11, 1990, pp. 1919, 1920.

[26]Majamaki, A. J., "Passive Mixing Control via Lobed Injectors in High Speed Flow," Ph.D. Dissertation, Dept. of Mechanical and Aerospace Engineering, Univ. of California, Los Angeles, 2001.

[27]Tew, D. E., "Streamwise Vorticity Enhanced Compressible Mixing Downstream of Lobed Mixers," Ph.D. Dissertation, Dept. of Aeronautics and Astronautics, Massachusetts Inst. of Technology, Cambridge, MA, 1997.

[28]Hall, J. L., Dimotakis, P. E., and Rosemann, H., "Experiments in Nonreacting Compressible Shear Layers," *AIAA Journal*, Vol. 31, No. 12, 1993, pp. 2247–2254.

[29]Selerland, T., and Karagozian, A. R., "Ignition, Burning, and Extinction of a Strained Fuel Strip with Complex Kinetics," *Combustion Science and Technology*, Vol. 131, No. 1–6, 1998, pp. 251–276.

I. Gokalp
Associate Editor